ABSTRACT

Title of Document:	MODELING OF A SINGLE-PHASE LIQUID COOLING SYSTEM FOR POWER ELECTRONICS APPLICATIONS
	Douglas John DeVoto, Master of Science, 2010
Directed By:	Associate Professor F. Patrick McCluskey Department of Mechanical Engineering

This work investigates the reliability of a single-phase, liquid cooling system used for the thermal management of a medium power level converter system. The system utilizes a plastic insert cold plate design to provide even cooling over the backside of a power electronics device by directing coolant through parallel serpentine channels. Material selection and compression set testing evaluated suitable elastomers for seals and polymers for the plastic insert. Computational fluid dynamics software was used to evaluate the thermal performance of the cooling system under ideal conditions as well as various wear out conditions (e.g. channel blockage, erosion of channel walls). Properties of used 50/50 ethylene glycol water coolant were evaluated to discover additional causes of reduced thermal performance. After completing the cooling system evaluation under initial and degraded conditions, the impact on a power module's operating temperature was correlated to an estimation of the device's reliability.

MODELING OF A SINGLE-PHASE LIQUID COOLING SYSTEM FOR POWER
ELECTRONICS APPLICATIONS

By

Douglas DeVoto

Thesis submitted to the Faculty of the Graduate School of the
University of Maryland, College Park, in partial fulfillment
of the requirements for the degree of
Master of Science
2010

Advisory Committee:
Dr. F. Patrick McCluskey, Chair and Advisor
Dr. Avram Bar-Cohen
Dr. Bongtae Han

Dedication

To my parents and family.

Acknowledgements

I would like to thank my advisor, Dr. McCluskey, for his time and guidance spent on this research. I would also like to thank my committee members for their input on how to improve the work presented.

I would also like to thank everyone in the McCluskey research group for their help and friendship over the past two years. Special thanks to Chandra, Vibhash, Kyle, Peter, and Robin for the time spent on research and classes together.

I would also like to thank CALCE for the use of its facilities and equipment.

I would finally like to thank my family for their love and support as I have pursued this degree, as they have always been there for me over the many years that have led to this point.

Table of Contents

List of Tables

List of Figures

Chapter 1: Introduction

Power electronics is the technology increasingly relied upon to manage and distribute the growing flow of power in a world dependent on electronics with ever higher performance. Power electronic components have been incorporated into a variety of applications ranging from energy generation and transmission to industrial automation and transportation. A power electronic device converts source electrical energy at a particular set of voltage, current, and frequency to another set better matched to the needs of a load, for both alternating current (AC) and direct current (DC) systems. The technical limits of power electronics are continually being stretched to reduce device size while increasing efficiency and reliability in more demanding environments.

Power electronics can be classified into the following four categories based on the type of conversion:

- Rectification – AC is transformed to DC; this most commonly occurs when any small electronic appliance (e.g. computer, television) is plugged into the mains supply.
- DC/AC inversion – DC is transformed to AC; an example would be the conversion of electrical energy from a battery to a variable speed AC motor in a hybrid electric vehicle.

- DC/DC conversion – A DC source is transformed to DC at a different voltage amplitude and possibly a reverse polarity; this is common in mobile electronic devices.

- AC/AC conversion – An AC source of a particular voltage amplitude and frequency is transformed to another amplitude and frequency to better meet the requirements of the load. This is common for the control of variable speed motor drives and the incorporation of renewable energy sources into the electrical grid.

These four conversion functions are executed by power converters, which are devices that include a control unit that monitors the load requirements and a power switch that regulates the power transmitted to the load. The control unit consists of integrated circuits for sensing the load demand and driving switching elements and is typically separate from the power switch in systems with high power ratings for thermal management purposes. The power switch in most applications utilizes silicon based power semiconductors for high efficiency and frequency performance compared to previously used mechanical switches. Newer systems are switching from silicon to silicon carbide for higher breakdown voltage and performance in a smaller size device.

Modern power converters are designed to minimize losses by efficiently passing energy through at low forward voltage in their on-state while efficiently restricting the passage of energy with a low leakage current in their off-state. In the short transient switching state between on and off states, switching losses are generated

and the power semiconductors heat up, with losses increasing with switching

frequency. To ensure a reliable converter, a cooling system must extract these heat

losses to limit temperature increases in the semiconductor device that would

jeopardize reliability and performance, specifically keeping the device from

exceeding its maximum operating temperature. A variety of power semiconductor

devices have been developed, each intended to operate most efficiency over a subset

of power ranges and switching frequencies. These are summarized in Table 1 [1].

Power converters in the range of several megawatts or higher use silicon-controlled

rectifiers (SCRs, thyristors) or gate turn-off thyristors (GTOs) and diodes. These

power ranges are typical for power distribution or large motor drive applications.

Insulated gate bipolar transistors (IGBTs) and diodes are used in medium power

applications such as traction drive systems for locomotives, motor control in hybrid

and electric vehicles, and power regulation for renewable energy sources. Lower

power applications generally use power metal-oxide-semiconductor field-effect

transistors (MOSFETs).

Table 1. Power range of typical power electronic converters.

Power Electronic Converter	Power Range	Switching Frequency Range	Application Examples
Light-triggered thyristor	Top end of power range: >1 GW	10 – 100 Hz	High voltage DC lines
GTO	High power range: 10 MW	100 – 500 Hz	Large power supplies, large motor control
IGBT	Middle to high power range: 1 – 10 MW	1 – 5 kHz	Traction drive for trains at several MW, motor control in industry, hybrid electric vehicles (HEVs)
Power MOSFET	Low end power range: 10 kW	100 kHz and higher	Computer power supply, RADAR

The focus of this research has been to evaluate the reliability and thermal performance of an IGBT based power electronic converter and an associated cooling system. Industry trends will push future converter designs to operate at higher heat fluxes and temperatures while reducing volume, switching losses and increasing reliability. The design approach to reach these goals is to evaluate new materials for use in the converters and improve heat rejection performance from the power electronics with more advanced cooling system technologies.

Chapter 2: Prior Work

This chapter outlines the results of prior work in the packaging of IGBT power electronic converters and associated reliability models for known failure mechanisms.

2.1   Power Electronics Packaging

Increasing power density levels for power electronic systems in energy and transportation applications continue to place higher demands on thermal management designs. An illustration of a general power electronic module is shown in Figure 1.
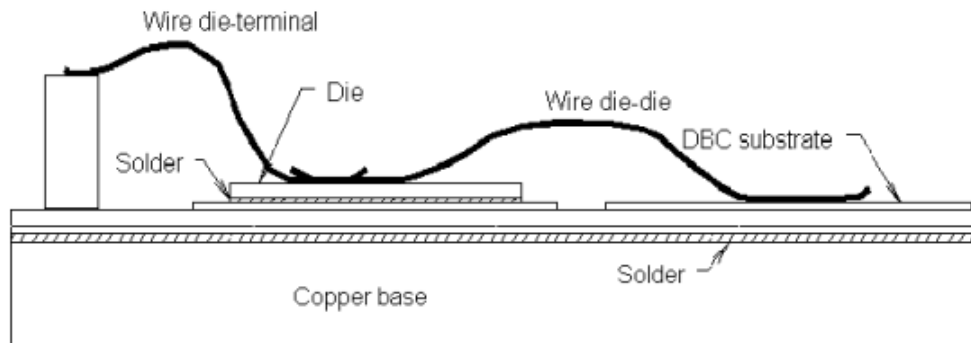
Figure 1. Cross-section of a power electronics module.

Thick aluminum wires capable of high current loads are bonded to silicon die surfaces. Each die is connected to a DBC (Direct Bonded Copper) ceramic substrate by a solder. The DBC itself is made by bonding copper film to a ceramic substrate at a temperature between 1065-1085 ˚C to form a copper-copper oxide-ceramic eutectic joint [3]. Alumina (Al_2O_3) is the most commonly used ceramic for a substrate material and manufacturing it has become a mature technology. However, its low thermal conductivity (24 W/m-K at 96% to 33 W/m-K at 99%) and thermal

expansion mismatch with silicon (6.0 to 7.2 ppm/K, for Al_2O_3, 2.8 ppm/K for Si) has caused other materials to be developed for high power semiconductor applications. Aluminum Nitride (AlN) has a thermal conductivity 4.5 to 7.5 times that of alumina (150-180 W/m-K) and a coefficient of thermal expansion (CTE) closer to silicon (4.6 ppm/K) but it is more expensive (10x) [4]. A thick copper base plate is also joined by solder to the backside of the DBC. A heat sink or other thermal management device is attached to the copper base plate to maintain the power electronic module within acceptable operating temperatures. A plastic enclosure protects the IGBTs and diodes from the environment and a silicone gel encapsulant provides an additional layer of protection from moisture and chemicals along with providing mechanical support and electrical isolation for the wirebonds. A typical power module with its plastic enclosure removed is pictured in Figure 2.
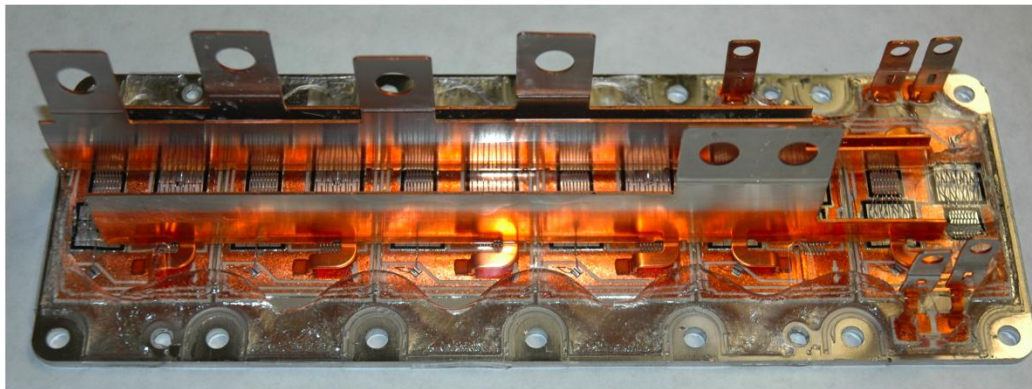
Figure 2. Disassembled power module.

An inverter assembly for an automotive application shows the power electronics devices and their associated driver board and controller removed from their protective enclosure in Figure 3. The cold plate that thermally manages the power electrics is also pictured [2].
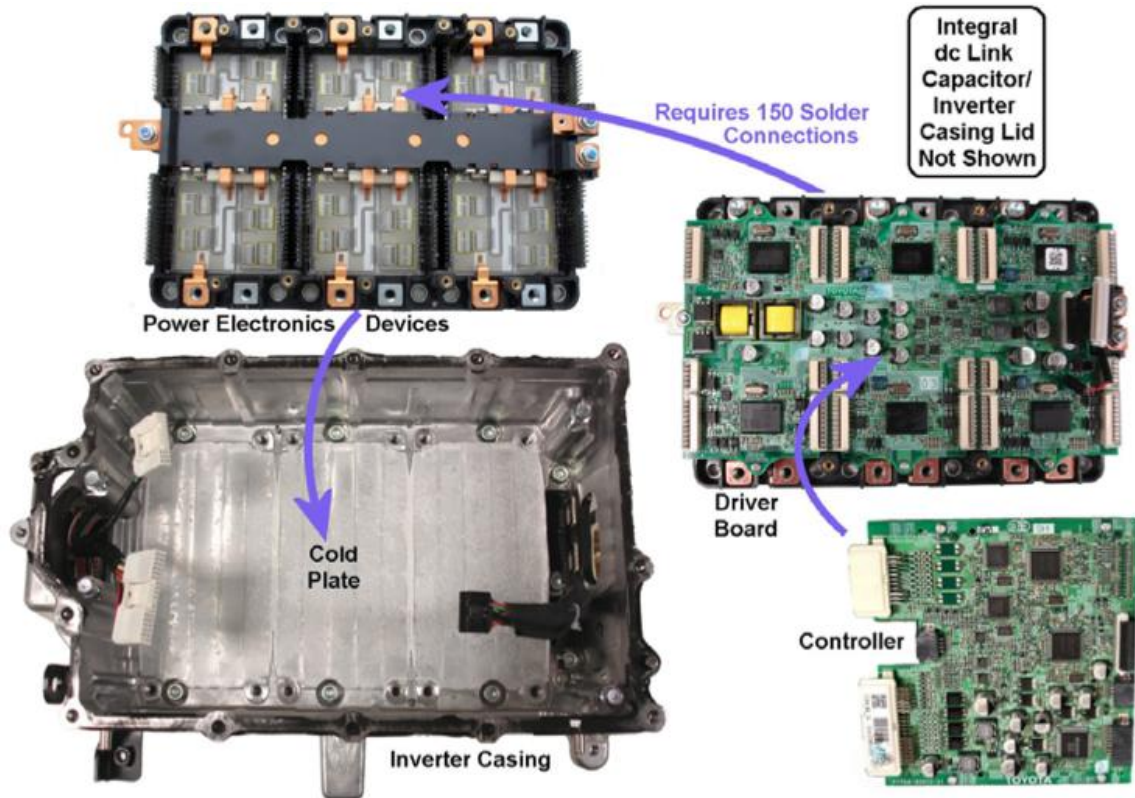
Figure 3. Automotive inverter assembly.

2.2 Power Electronics Failure Mechanisms

Several dominant failure locations have been identified in power electronic modules, specifically the bond wires, die attach, and ceramic substrate [5]. Failures are likely to occur as a result of operational loads inducing thermo-mechanical stresses/strains in the package. Bond wires exhibit flexure fatigue failures at the heel during thermal cycling if they are not encapsulated. Shear stresses at the interface with the bond pad can cause bond liftoff. A CTE mismatch between the die component and solder, and solder and substrate, will cause stresses and strains in the die attach material that can result in die attach fatigue upon repeated thermal cycling. Thermal cycling also causes fatigue failure in the ceramic substrate from the local CTE mismatch between copper and ceramic (e.g. Al_2O_3) [3].

Additional failure mechanisms can occur from the cracking of copper leads bonded to the DBC substrate. In the ultrasonic welding process, high frequency vibrations and moderate pressure are applied on two metal parts to form a weld between both surfaces [6]. If the manufacturing process does not completely bond the two copper surfaces, micro-cracks will be present along the interface, causing a weaker than designed weld. The CTE of the module's outer plastic enclosure can also cause stress/strain reversals resulting in lead fatigue failure.

Chapter 3: Cooling Systems for Power Electronics

3.1   Selection of Cooling System Technology

Many of the power module failures discussed can occur from exposure to temperature extremes or from thermal cycling. Power electronic devices have continued to increase in power limits and heat flux demands, exceeding the capabilities of air cooling systems. A gradual shift has occurred for accepting liquid cooling systems as favorable and necessary thermal management solutions.

In an air cooling system, a heat spreader dissipates and transfers heat from a device to an air cooled fin structure, or heat sink. As heat fluxes from power electronics increase, the effectiveness of the spreader to laterally distribute heat across the heat sink decreases to the extent where liquid cooling systems offer many advantages [7]. Liquid systems are capable of providing thermal management solutions for high flux conditions that require less space and power demand, and operate at reduced noise levels when compared to air cooling systems. A variety of cold plate designs have been developed to meet a range of heat dissipation requirements through various techniques, including jet impingement, spray, pool boiling, flow boiling, and single-phase liquid. Several single-phase liquid cold plate configurations allow for device cooling at different ranges of power applications. For low power applications, a coolant tube network is attached, by solder or thermal epoxy, to a cold plate substrate, typically made of copper or aluminum. To reduce thermal resistance, tubing can be replaced by drilling holes into the cold plate substrate. Caps and plugs

in the holes are inserted to achieve the desired flow path. For higher heat fluxes, the

design of the channels is improved from simple tubes to machined pathways. The

width and pattern of the channels can be varied to address the needs of the device

location and heat flux levels. A cover plate is soldered or bolted over the machined

base plate to complete the cold plate. Channel performance can be further improved

by inserting pocked fins to increase surface area and the local heat transfer

coefficient.
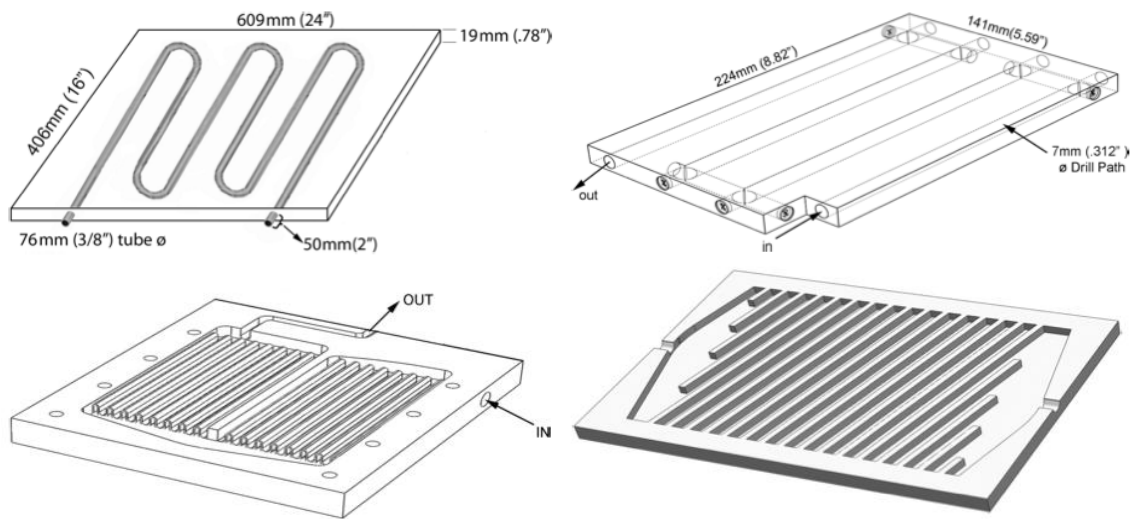
Figure 4. Cold plates. Clockwise from top left: formed tube, drilled, machined channel, and finned [7].

The described cold plate designs, also pictured in Figure 4, are several available

solutions when designing a thermal management system that meets specified

parameters of device power dissipation and location, inlet coolant temperature,

flow rate, and pressure drop. An example of one solution for an inverter assembly in

a hybrid electric vehicle is shown in Figure 5. A simple serpentine channel design is

improved by adding fins that correlate to power electronics arrangement.
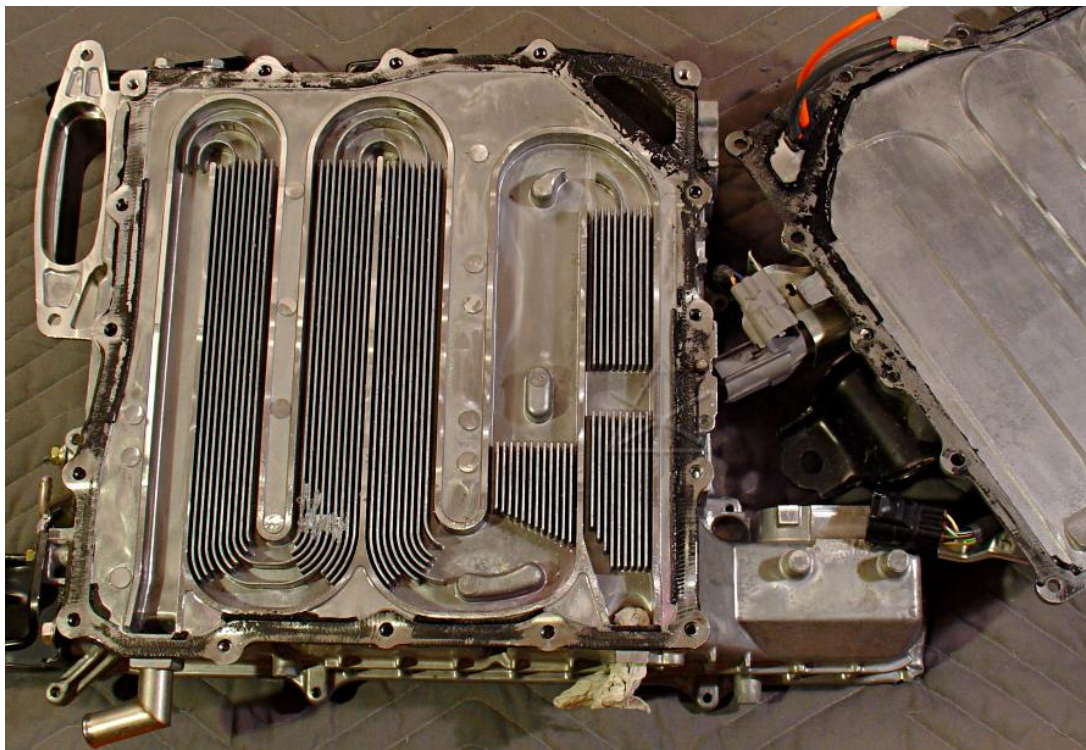
Figure 5. Automotive cold plate design [8].

3.2   Liquid Impingement Cooling System Study

One commonality among the aforementioned cold plates is the reliance upon a

metal, typically copper or aluminum, to be fabricated or machined to form the liquid

cooling designs. A novel alternative in liquid cooling systems is to direct coolant

through a series of meandering cells by the use of a plastic insert, shown in Figure 6.
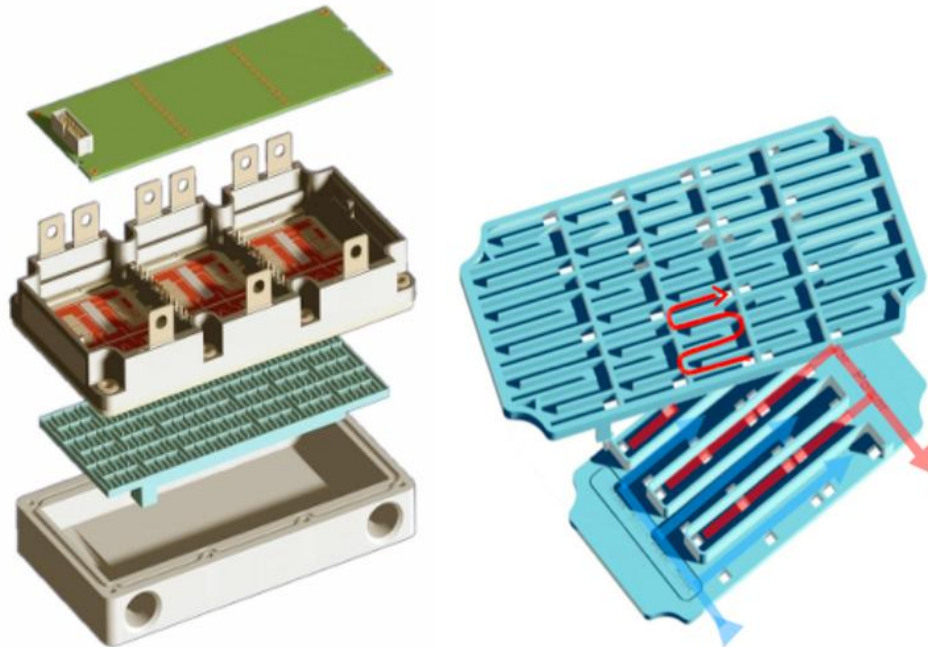
Figure 6. Plastic insert cold plate design (left) and insert (right).

Coolant enters a metal base plate that is directly bolted to the back side of a power electronics module. The plastic insert contains several wide channels with closed ends that direct the coolant into a series of meandering cells. While in the cells, the coolant is in direct contact with the base plate of the power electronics module. Coolant then exits the cells into a second set of wide channels that direct the fluid to the cold plate's outlet location. The advantage of the plastic insert is that the series of individual cells prevents a large thermal gradient from forming along the cold plate; even cooling is achieved over the entire base plate surface. An example of uneven cooling is shown in Figure 7 from a traditional cold plate design. Coolant enters from the bottom left and adequately cools the left side of a power electronics module. The coolant rises in temperature as it passes through the cold plate and becomes less effective at cooling a module towards its exit in the top right location. An additional focus must be taken to ensure that IBGT and diode pairs stay within

their maximum temperature design parameters, regardless of their placement over a cold plate with uneven cooling.
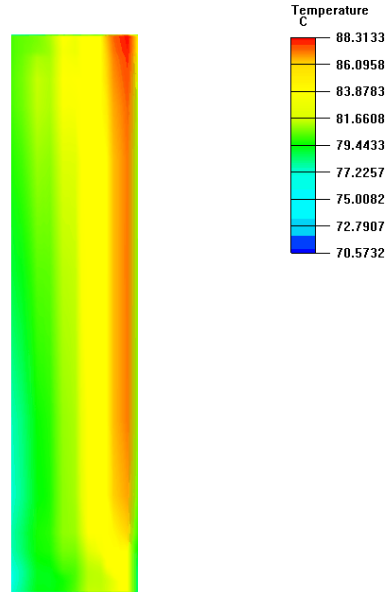
Figure 7. Traditional cold plate cooling of a module baseplate.

The low cost of injection molding of plastic components also allows for a plastic-insert cold plate design to be specifically tailored to various thermal management demands [9]. Reliability in the liquid cooling system, particularly for a novel design, must be evaluated as closely as the power module; therefore possible wear out and fouling conditions have been explored. After a material evaluation of the plastic insert and elastomer seal, a model of the cold plate design was created to evaluate baseline performance as well as likely degradation conditions. Used coolant was also analyzed for other possible performance degradations of the cold plate.

Chapter 4: Experimental Procedure

4.1 Material Evaluation

Two key materials in the described cooling system are the plastic insert and

elastomer seal. Alteration or degradation of either material could lead to a reduction

in cooling performance or ultimately failure of the cooling system. Each material

was evaluated under several chemical and thermal criteria.

4.1.1 Seal Analysis

A variety of environmental conditions must be evaluated in the material selection of

a seal or gasket design. An understanding of the thermal and mechanical loads, as

well as chemical exposure will ensure a proper seal material is selected. The

consequences of misevaluating a seal's performance requirements can create a

failure in three ways, a change in appearance, contamination, or leakage [11]. The

most significant failure, leakage, could reduce the performance of a cooling system

to the extent that a converter unit would need to be turned off, or else face failure

itself by components exceeding temperature limitations.

The following compounds represent the most common selections used in industry

for any sealant application:

- Nitrile/ Buna-N-nitrile (NBR) – Nitrile is a copolymer of butadiene and
acrylonitrile, and is the most common material for o-rings. Raising the
concentration of acrylonitrile increases resistance to petroleum but also

decreases low temperature flexibility [12]. Nitrile compound seals do not perform well with ozone, sunlight, or exposure to weather.

- Polychloroprene / Neoprene (CR) – Polychloroprene is produced by the polymerization of chloroprene and is characterized by having good resistance from the sun, ozone, weather, and oils. A foamed compound version can be used as an insulation material [13].

- Ethylene propylene diene (EPDM, EPM) – Ethylene propylene diene has excellent chemical resistance but should not be used with petroleum oil applications. It has excellent weather resistance, low temperature flexibility, and has been used as a seal material in water systems, brake, and automotive cooling systems.

- Silicone (VMQ) - Silicone is a semi-organic elastomer that is resistant to temperature extremes and also to compression set. It is limited to static seals due to its poor friction properties and abrasion resistance.

- Fluorosilicone (FVMQ) - Fluorosilicone exhibits the same properties of silicone but is also resistant to petroleum oils and hydrocarbon fuels.

- Fluoroelastomer, Aflas, Viton (FKM) – Fluoroelastomer compounds can operate far longer than nitrile based seals and are exceptionally resistant to chemicals, heat, ozone, sunlight and exposure to weather. O-rings can operate continuously up to 204°C and can withstand some excursions to 315°C. The compound loses some of its flexibility at lower temperatures and is more expensive to produce than other elastomers.

- Perfluoroelastomer, Kalrez, Simriz, Chemraz (FFKM) –

  Perfluoroelastomer seals, also commonly known by the trade names

  Kalrez®, Simriz® and Chemraz®, exhibit strong chemical resistance and

  thermal stability to allow them to last longer than other elastomers [14].

  This is achieved by their chemical structure of replacing hydrogen atoms

  with fluorine atoms. They are compatible with over 1,800 chemicals and

  retain elasticity when exposed to temperatures up to 316°C.

  Perfluoroelastomer seals have been used extensively in oilfield and other

  subsurface drilling industries, as well as in demanding thermal and

  chemical environments for the aerospace, semiconductor, food and

  pharmaceutical industries. However they are expensive and difficult to

  produce.

These elastomers were evaluated under several chemical and thermal constraints

for an o-ring seal in a cold plate [15]–[18]. A summary is provided in Table 2. For

chemical compatibility, 1 = Excellent, 2 = Good, 3 = Fair, and 4 = Not Recommended.

Table 2. Elastomer material evaluation.

	Ethylene Glycol	Water (>80°C)	Max. Temp. (°C)	Low Temp. (°C)	Cost
Nitrile (Buna-N)	1	1	121	-25 to -30	1:1-2
Polychloroprene	1	3	105	-50	1:2
Ethylene Propylene Diene	1	1	150	-54	1:1
Silicone	1	1	204	-85 to -125	1:2.3-6.7
Fluorosilicone	1	1	175	-65	1:19-27
Fluoroelastomer	1	1	204	-8 to -30	1:10.7-16
Perfluoroelastomer	1	1	316	-8	1:16

During its service life, the o-ring seal must not degrade in performance when in contact with other chemicals found in its environment. This requirement is critical in hot environments when a long service life is desired. Evaluations of the most common elastomers have documented their chemical resistance to over 1,600 chemicals and fluids [15]. These ratings were previously established through volume swell resistance from laboratory immersion testing, laboratory aging testing, and field results. Of the elastomers used for seals and o-rings, most have excellent performance when in contact with ethylene glycol and high temperature water. Chemical attack can target fillers in the elastomers as well as cross-linking, leading to degradation in the form of swelling or embrittlement. The properties of an elastomer will vary if it is required to operate in conditions with varying temperatures. Low temperatures can increase retraction, stiffness, brittleness, and crystallization of an elastomer, but are typically reversible. TR-10 is the temperature where an elastomer will retract by 10%. The high temperature limit is defined for an elastomer at a loss of 30-50% of physical properties. High temperature limits can cause irreversible changes in the elastomer's cross-linking that lead to permanent degradation. A seal in a cold plate that can be exposed to harsh environmental conditions must be able to withstand temperatures as low as -40 ℃ and as high as 125 ℃. Of the elastomers described, ethylene propylene diene, silicone, and fluorosilicone meet the requirements for chemical and thermal compatibility. If compatibility with fuel oils is an additional concern, the selection can be narrowed to fluorosilicone as the most appropriate material.

4.1.2 Polymer Insert Analysis

A similar chemical and thermal evaluation from literature was performed over a variety of common polymers for inserts, listed in Table 3. Each material was rated for its compatibility with ethylene glycol, fuel oils, and water, where A = Excellent, no effect, B = Good, minor effect, R = Resistant, C = Fair, moderate effect, and U = Poor, severe effect. The materials were also evaluated for their thermal performance by their maximum continuous operating temperature and their heat deflection temperature.

Table 3. Polymer inset material evaluation [19]-[22].

	Ethylene Glycol	Fuel Oils	Water Absorption 24H (%)	Max. Temp. (°C)	Heat Deflection Temp. (°C)	CTE (10^{-5}/°C)	Thermal Conductivity (W/m-K)
ABS	A	U	0.3	60	102	9.54	0.19 to 0.33
Acetal	B	A	0.2	82	104 to 121	9.72	0.23 to 0.36
CPVF	A	A	0.04	93	103	6.66	0.14
Teflon (PTFE, FEP)	A	B	<0.01	260	65	10.8 to 13.5	0.25
Nylon 6	R	R	0.3 to 0.5	85 to 150	93	6.3	0.25
HDPE	R	R	0	82	82	10.8	0.46 to 0.52
PEEK	A	B	0.01	250	160	4.68	0.25
Polyamide-Imide	A	A	0.4	260	271 to 278	2.52 to 4.68	0.26 to 0.54
Polyphenylene Sulfide (PPS)	A	A	0.01	218	121	5.04	0.29
Polypropylene	A	A	0.01 to 0.02	82	52	11.16 to 11.88	0.11 to 0.12
PVC	R	R	0	60	80	10.98	0.13
PVDF	A	B	0.03	130 to 150	110	11.88	0.17

Several materials were found to show no effect when in contact with ethylene glycol, minor to no effect with fuel oils, and only marginal absorption of water when submerged for 24 hours. The heat deflection temperature of a polymer is the temperature at which a sample deflects a defined amount, when a defined

temperature and pressure is applied. Tests are conducted under the ASTM D-648 standard, typically at 0.46 MPa or 1.8 MPa. Temperature values listed in Table 3 were measured at 1.8 MPa. It was desired that the acceptable materials would show minimal deflection at temperatures up to 100 ℃. While providing a method to compare loading of different resins, the heat deflection temperature does not indicate operating temperatures. Resins should also be kept below their maximum continuous operating temperatures, defined as the temperature where a decrease in tensile strength can be measured after continuous use for 5,000-20,000 hours [22]. For the cold plate application, 100 ℃ was also chosen as the maximum continuous operating temperature. For the described temperature and chemical requirements, polyether ether ketone (PEEK), polyphenylene sulfide, and polyvinylidene fluoride (PVDF) meet the design requirements.

4.2   Compression Set Testing

In addition to the material evaluation of the plastic insert and elastomer seal, compression set testing was completed on seal samples to measure any effects when compressed in air and ethylene glycol. Compression set describes the deformation that remains after a stress is removed. Compression set tests for materials are defined in ASTM D-395 and are categorized by two methods. Method A applies a constant force to a specimen for a specific time and temperature. Method B compresses a specimen 25% for a specific time and temperature. Both methods allow the material to recover for 30 minutes before the percentage of deflection is measured [23]. It is not required for a material to recover completely to be an effective seal, particularly for constant compression seals. However, a material with

excessive compression set in an environment with excessive compression or elevated temperature will lead to a flat-sided cross-section and introduce the possibility of leakage. An example of compression set of an o-ring seal is shown in Figure 8.

Figure 8. O-ring compression set [21].

Compression set is dependent on temperature, with higher temperatures accelerating the amount of deformation, shown in Figure 9.
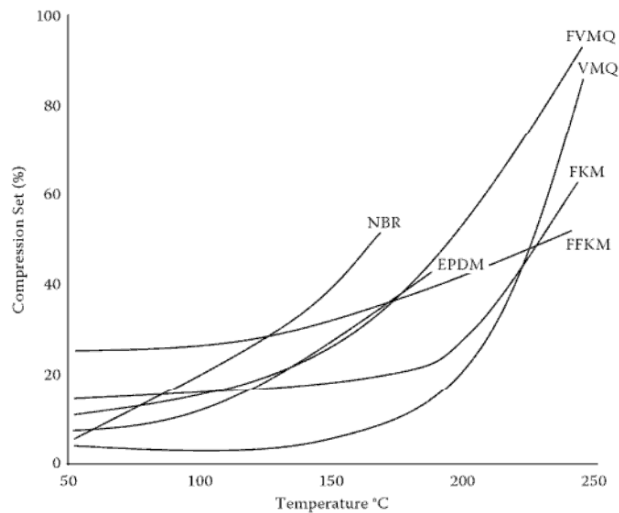
Figure 9. Compression set of various sealing elastomers [24].

A compression set test fixture was constructed to the ASTM D-395 Method B standard. Three aluminum plates were machined to have a matching hole pattern for bolts to compress the assembly in each corner. Between each plate, metal spacers were machined to the appropriate thickness to compress seal samples to

75% of their original thickness. For a test, seal samples and spacers were first placed between the aluminum plates. Then the assembly was compressed with four bolts and placed in a container of ethylene glycol. The compression set assembly remained submerged in the liquid for 72 hours at various temperatures. The assembly design is pictured in Figure 10.
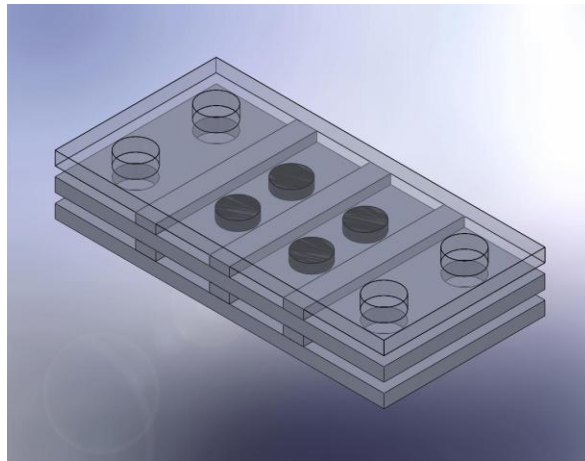
Figure 10. Compression set assembly.

EPDM 70A durometer was used as the rubber material for all test conditions. Results were completed twice at room temperature in the glycol solution and in air. Additional tests were conducted at 60, 80, and 100 ˚C. A summary of the test results is shown in Figure 12 and Figure 12.
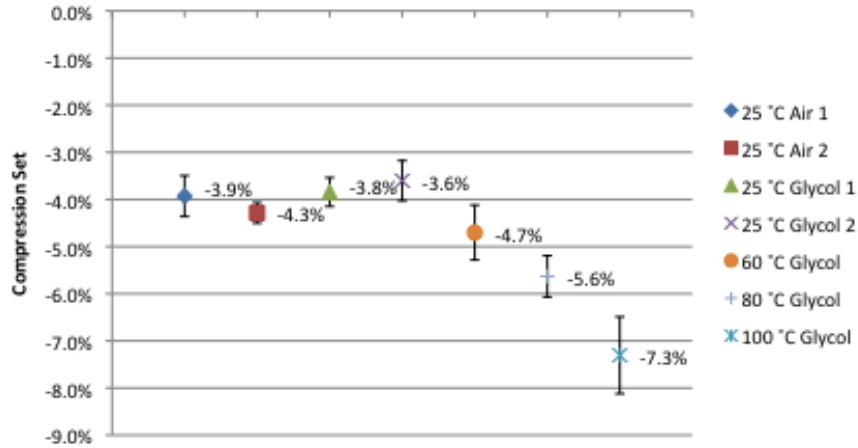
Figure 11. EPDM compression set results.
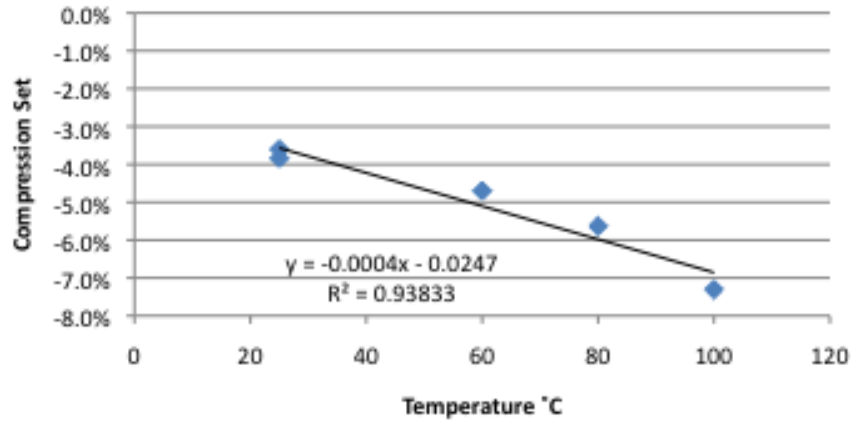
Figure 12. Compression set vs. temperature.

EPDM results at 25 ℃ showed slightly more compression set in air than submerged

in coolant. Results over a 25 ℃ to 100 ℃ range showed an increasing level of

compression set with increasing temperature. Compression set results in the glycol

coolant were found to correlate linearly with temperature to R^2 = 0.94. These results

were sufficiently small to alleviate concerns about leakage and compare closely to

documented compression set levels for EPDM within this temperature range [24].
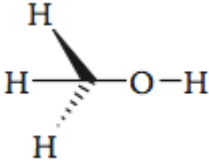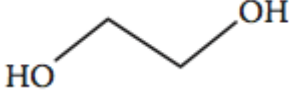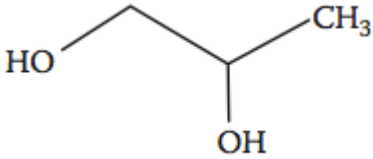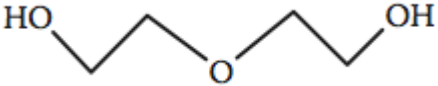
4.3   Coolant Fluid

A common coolant fluid was analyzed after several years of operation to establish if additional degradation conditions can develop. A description of the compound and its evaluation follows.

4.3.1   Compound Description

Water was the first material used as a cooling fluid but corrosion issues, especially at high voltages, and limited operating range led to the development of alternative coolants. Typical liquid cooling systems for automotive or electrical power generation applications use a mixture of de-ionized water with an oxide inhibitor, such as antifreeze [10]. In 1926, ethylene glycol became available as "permanent antifreeze" and serves as a cryoprotectant to water by reducing the freezing point of the mixture. Ethylene glycol also has a higher boiling point and replaced other compounds such as methanol. It is a poisonous substance that forms calcium oxalate crystals in the kidneys and causes acute renal failure. Denatonium benzoate is added as a bittering agent to dissuade ingestion. Propylene glycol is considered a nontoxic antifreeze and is used primarily in the food processing industry. The compound breaks down more easily than ethylene glycol and yields organic acids [24]. A summary of various coolant properties for the compounds is shown in Table 4.

Table 4. Various coolant properties [24].

Compound	Boiling Point (°C)	Mass (g/mol)	Density (g/cc)	Structure
Methanol	64.7	32.04	0.79	
Ethylene Glycol	197.3	62.07	1.11	
Propylene Glycol	188.2	79.06	1.04	
Diethylene Glycol	244	106.12	1.12	

Antifreeze is typically diluted to a 1:1 glycol to water mixture, providing freeze protection down to -40 °C. Corrosion-inhibiting compounds are added and a dye is added for identification. Modern coolant solutions incorporate a mixture of compounds to achieve longer life performance with the use of organic acid technology (OAT) antifreezes such as Dex-cool. In addition to glycols, an OAT antifreeze includes a percentage of the additive 2-Ethylhexanoate, as shown in Table 5.

Table 5. OAT coolant properties [25].

Physical	
Color	Orange
Odor	Sweet to faint
pH	8.0-8.6
Vapor Pressure	<0.01 mm Hg at 20 ˚C
Boiling Point	108.9 ˚C
Freezing Point	-36.7 ˚C
Flash Point	127 ˚C
Autoignition Temperature	400 ˚C
Specific Gravity	1.12 at 15.6 ˚C
Viscosity	8 cSt at 40 ˚C
Chemical	
Ethylene Glycol	80 – 96.99 % weight
Diethylene Glycol	1 – 4.99 % weight
2-Ethylhexanoate	1 – 4.99 % weight
Water	1 – 2.99 % weight

Ethylhexanoate, along with sebacic acid and tolyltriazole, are used as additives that combine with metal constituents within a coolant loop. Their structure is displayed in Figure 13.
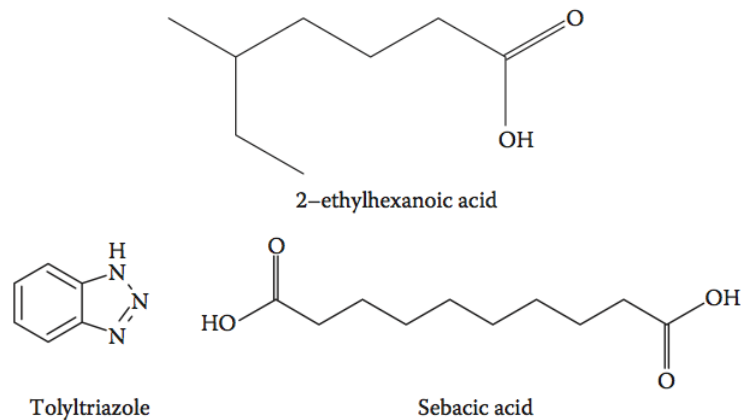
Figure 13. Structure of OAT additives.

Organic acid additives do not deplete as quickly as inorganic inhibitors and in addition to longer life, have lower alkalinity, no silicates, nitrates, amines, borates,

or nitrates, and are biodegradable. Havoline originally patented OAT coolant but it has since expanded to a variety of manufacturers [24].

4.3.2 Degradation Analysis

Used OAT coolant by Texaco/ Havoline was obtained from the liquid cooling systems of several 3.0 MW wind turbines. Maintenance records showed that the coolant had been in operation for over three years. An analysis was conducted to evaluate if the used coolant had deviated outside of acceptable parameters compared with new coolant. Samples were taken at several locations within two separate coolant loops. The first loop cools the generator, converter, and hydraulic systems while the second loop cools the gear oil system. The first coolant loop is the primary focus area because it includes the converter system. Simplified diagrams of both coolant loops are shown in Figure 14 and Figure 15.
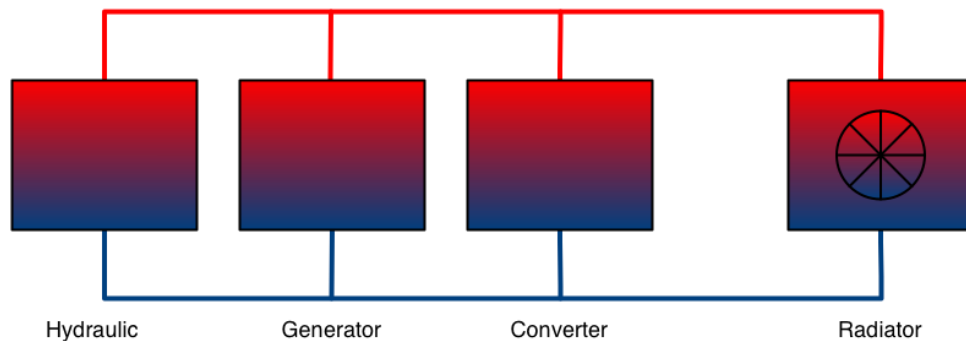
Figure 14. Generator, converter, and hydraulic cooling system.
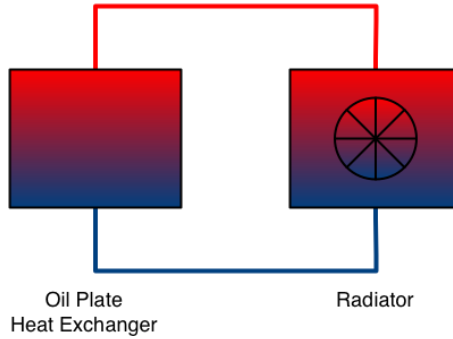
Figure 15. Gear oil cooling system.

Coolant samples 1, 2, and 3 were taken from the generator drain, VCRS (converter) drain, and generator circuit radiator drain, respectively, in the first cooling system loop. Samples 4 and 5 were collected from a coolant pump and the gear circuit radiator. A comparison of the used coolant was made with new coolant over a variety of physical properties, including color change, density, pH, electrical conductivity, viscosity, and glycol percentage. A summary of results is shown in Table 6 below, followed by a description of the experimental procedures and a discussion of results.

Table 6. Used coolant properties.

	Sample	Density (kg/L)	pH	Conductivity (mS/cm)	Kinematic Viscosity (cSt)	Freezing Point (°C)	Ethylene Glycol %	Boiling Point (°C)
New	-	1.05	8.0	2.32	3.42	-45.0	56.3	109.6
Turbine 1	1	1.07	7.0	2.41	4.59	-49.0	57.8	110.0
	2	1.07	7.0	2.44		-48.5	57.7	110.0
	3	1.06	7.0	2.42		-48.5	57.7	110.0
	4	1.08	8.0	2.20	6.11	-55.0	59.2	110.5
	5	1.03	8.0	2.22		-55.0	59.2	110.5
Turbine 2	3	1.06	7.5	2.35	4.86	-47.0	57.1	109.8
	5	1.05	7.5	2.78	3.24	-29.5	45.3	106.7
Turbine 3	1	1.06	7.5	1.89	9.15	-60.0	59.5	110.5
	2	1.06	7.5	1.88		-60.0	59.5	110.5
	3	1.07	7.5	1.86		-60.0	59.5	110.5
	4	1.06	8.0	1.93	6.75	-55.0	59.2	110.5
	5	1.06	8.0	1.95		-55.0	59.2	110.5

Color Change

Visual inspection of coolant samples indicated a distinct color change from new coolant. Samples 4 and 5 from each pad became slightly darker orange while samples 1, 2, and 3 were a darker red color. Small undissolved particles could also be seen in samples with an orange color. Particles could not be seen in darker red samples. A visual comparison of the samples is shown in Figure 16.
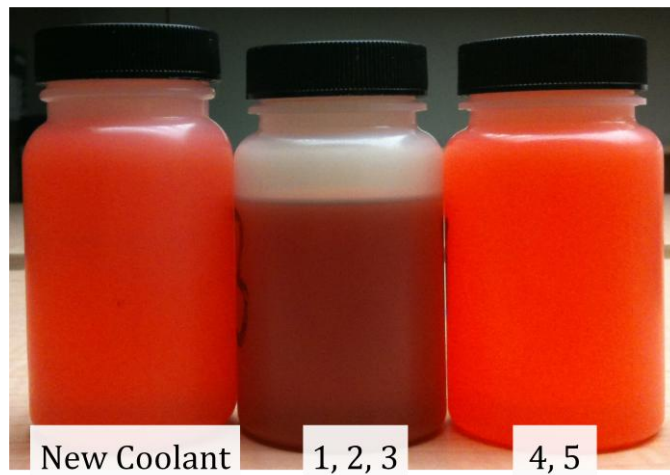
Figure 16. Color comparison of coolant.

Density

75 mL samples of coolant were dispensed into glass beakers. The respective mass of each sample was recorded using an electronic scale, with the beaker weight subtracted. Used coolant was found to have a marginally higher density than new coolant, indicating an increased percentage in glycol percentage.

pH

Coolant samples were each measured for pH with the use of test strips. The test strips were calibrated to have a color correspond to each pH level, from 1 - 14. A test strip color between two pH color levels was recorded as the lower pH + 0.5. pH.

Levels between 8.5 and 11 are typical for conventional coolants while long life coolant has levels between 7 and 9. pH levels of used coolant were slightly lower than new coolant but were still acceptable and would not be a concern for causing corrosion issues. High pH levels may be an indication of a blend of conventional and long life coolants or excessive additive treatment while low pH levels may highlight a local hot spot of air leak in the cooling system [26].

Conductivity

Conductivity levels were measured with a lab conductivity instrument. Deionized (DI) water was measured throughout the experiment as a control at 0.02 mS/cm. Conductivity levels above 7.5 mS/cm can lead to corrosion in the cooling system and reduce performance of some inhibitors, but no samples approached this limit.

Kinematic Viscosity

Viscosities of coolant samples were measured with a Cannon-Fenske Routine viscometer. New coolant was found to have a kinematic viscosity of 3.42 CentiStokes. For comparison, the viscosity of ethylene glycol is 17.8 cSt and DI water is 1.0038 cSt, indicating increased glycol percentage. Viscosity values of the coolant are acceptable but should not exceed limits specified by pump manufacturers.

Freezing Point/ Ethylene Glycol %/ Boiling Point

The freezing point of coolant samples was measured with a handheld refractometer. Several drops of coolant were placed on a prism; more concentrated coolant bent the light more and values were obtained from a calibrated scale. An example of a reading is shown in Figure 17.
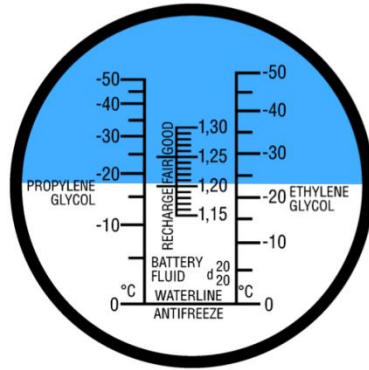
Figure 17. Example refractometer reading.

Results found that the used coolant samples had freezing points significantly lower

than new coolant, correlating with the increased density and viscosity

measurements. The ratio of glycol to water directly affects the freezing point of the

coolant mixture, and freezing points at various ratios were obtained from literature

[29]. The data was plotted, shown in Figure 18, and a curve fit was found to be

$$y = -0.0161x^2 - 1.9063x + 3.078 \qquad\qquad (1)$$

where y is the ethylene glycol percentage in the solution and x is the freezing point

temperature in °C previously measured.

$$y = -0.0161x^2 - 1.9063x + 3.078$$

$$R^2 = 0.992$$
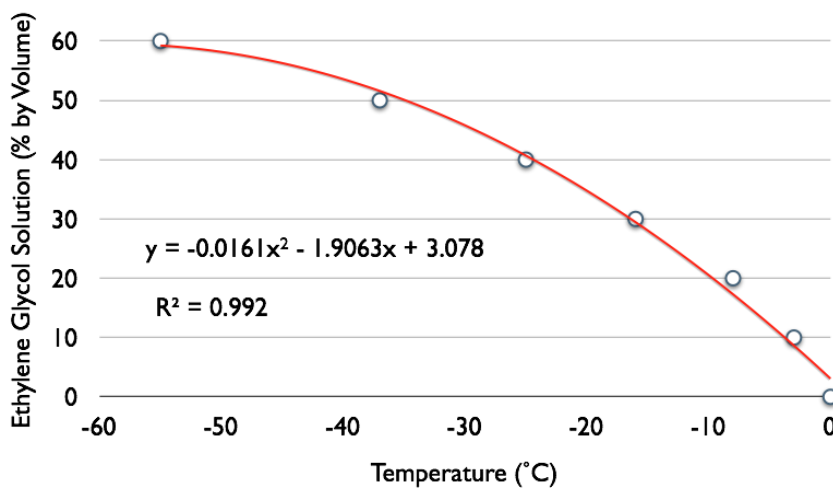
Figure 18. Glycol percentage as a function of freezing point.

The glycol concentrations in the used samples were found to be significantly higher

than the 50% specifications of the coolant, with many samples approaching 60%

glycol. A correlation similarly developed between the ethylene glycol percentage

and the coolant's boiling point was found to be

$$y = -0.0022x^2 - 0.0411x + 100.31 \qquad\qquad (2)$$

where y is the boiling point in $°C$ and x is the ethylene glycol percentage in the

solution. This relationship is again illustrated in Figure 19.
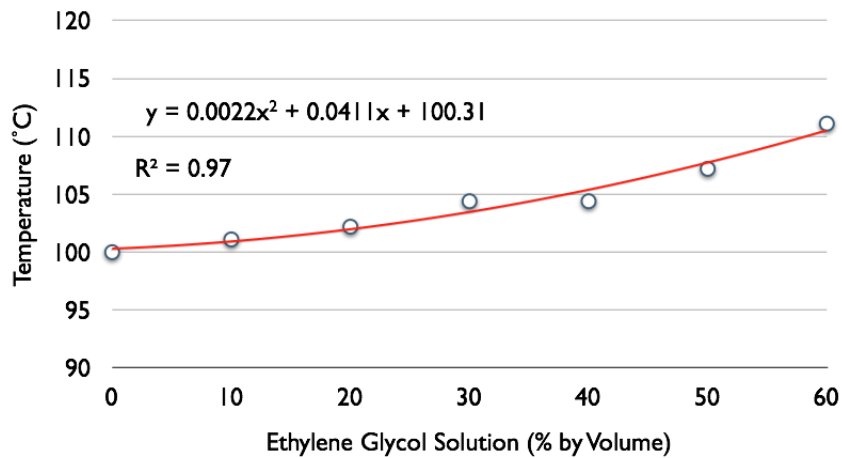
Figure 19. Boiling point as a function of glycol percentage.

While the boiling point varies slightly with higher glycol percentages, the heat

transfer capability of the coolant is diminished, requiring more fluid to be pumped

for an equivalent cooling ability. The impact of a 60% ethylene glycol solution as the

coolant is evaluated in the following reliability assessment as a possible degradation

condition. Overall, the elevated concentration of ethylene glycol in the coolant

samples was found to be the only material property out of design specifications.

Chapter 5: Reliability Assessment

Computer-aided engineering (CAE) software was used to model the thermal performance of a plastic-insert cold plate design. The cold plate was studied for effectiveness under optimal operating conditions, as well as under extended wear out or fouling conditions. A review of the software, model development, and results is provided in this chapter.

5.1   Software Background

A plastic-insert cold plate was modeled in the CAE software Icepak to allow for evaluation of the heat transfer and fluid flow simulations of the device under both optimal operating conditions and several degradation conditions. The Icepak software package includes several components to achieve results. Filters allow for importing of model geometry data from other computer-sided design (CAD) or CAE packages. This imported geometry, or geometry created in Icepak, is used to construct a model. Icepak creates a mesh for the model geometry and passes the mesh and model definition to its solver engine. The package uses FLUENT as its computational fluid dynamics (CFD) solver engine for both thermal and fluid-flow calculations [27]. After a solution is calculated, Icepak can be used to examine the results. The program structure is illustrated in Figure 20.
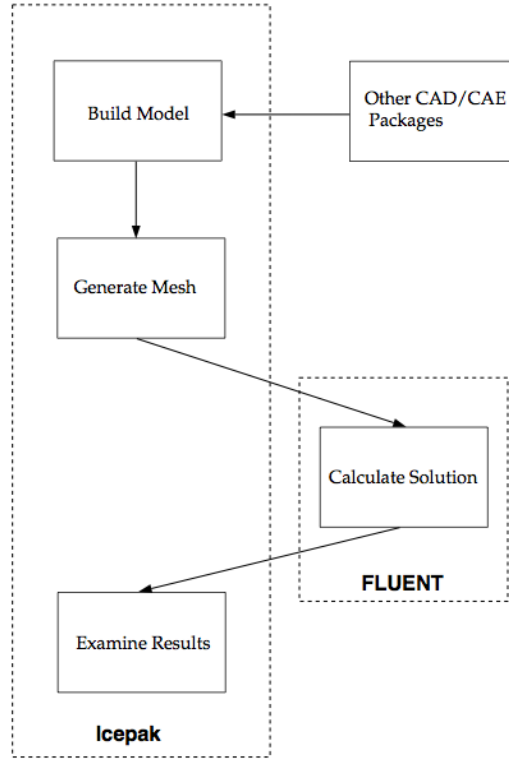
Figure 20. Icepak program structure.

Icepak solves the Navier-Stokes equations for transport of mass, momentum, and energy, as well as additional transport equations for turbulent flow with heat transfer. The equation for conservation of mass, or continuity equation, is as follows:

$$\frac{\partial \rho}{\partial t} + \nabla \cdot (\rho \vec{v}) = 0 \tag{3}$$

For an incompressible fluid, this equation simplifies to

$$\nabla \cdot \vec{v} = 0 \tag{4}$$

Transport of momentum in a non-accelerating reference frame is described by [28]

$$\frac{\partial \rho}{\partial t}(\rho \vec{v}) + \nabla \cdot (\rho \vec{v} \vec{v}) = -\nabla p + \nabla \cdot (\bar{\bar{\tau}}) + \rho \vec{g} + \vec{F} \tag{5}$$

33

where p is the static pressure, $\rho\vec{g}$ is the gravitational body force, and $\vec{F}$ contains

other source terms that may arise from resistances. The stress tensor $\bar{\bar{\tau}}$ is given by

$$\bar{\bar{\tau}} = \mu \left[(\nabla\vec{v} + \nabla\vec{v}^T) - \frac{2}{3}\nabla \cdot \vec{v}I \right] \tag{6}$$

where μ is the molecular viscosity, I is the unit tensor, and the second term on the

right-hand side is the effect of volume dilation [27].

The energy equation for a fluid region is defined as

$$\frac{\partial}{\partial t}(\rho h) + \nabla \cdot (\rho h\vec{v}) = \nabla \cdot [(k + k_t)\nabla T] + S_h \tag{7}$$

where h is sensible enthalpy, k is the molecular conductivity, k_t is the conductivity

due to turbulence, and S_h is the source term that includes any volumetric heat

sources. For conducting solid regions, a conduction equation is solved that includes

heat flux from conduction and volumetric heat sources within the solid:

$$\frac{\partial}{\partial t}(\rho h) = \nabla \cdot (k\nabla T) + S_h \tag{8}$$

where ρ is density, k is conductivity, T is temperature, and S_h is the volumetric heat

source. The conduction equation above is solved simultaneously with the energy

equation for the fluid region for a coupled conduction/ convection heat transfer

prediction [27].

Icepak includes eight turbulence models that balance computational time with

accuracy to calculate turbulent viscosity. A family of two-equation models has been

developed that allow the turbulent velocity and length scales to be independently

solved. An enhanced two-equation (standard k-ε with enhanced wall treatment)

model was chosen for its additional effort in calculating the flow in the near-wall region. The near-wall region can be further divided into three separate regions. The innermost layer, the viscous sublayer, can be considered to have a laminar flow and molecular viscosity dominates momentum and heat or mass transfer. The outer layer, the fully-turbulent layer, is dominated by turbulence. A transition region is affected equally by molecular viscosity and turbulence. The enhanced two-equation model divides a flow based on wall distance and the turbulent Reynolds number into a viscosity dominated laminar region and a fully-turbulent region. The enhanced wall functions used for the viscosity region are provided in greater detail in the Icepak User's Guide [27]. The turbulent region relies on transport equations for the turbulent kinetic energy (k) and its dissipation rate (ε) as follows:

$$\frac{\partial}{\partial t}(\rho k) + \frac{\partial}{\partial x_i}(\rho k u_i) = \frac{\partial}{\partial x_i}\left[\left(\mu + \frac{\mu_t}{\sigma_k}\right)\frac{\partial k}{\partial x_i}\right] + G_k + G_b - \rho\varepsilon \tag{9}$$

and

$$\frac{\partial}{\partial t}(\rho\varepsilon) + \frac{\partial}{\partial x_i}(\rho\varepsilon u_i) = \frac{\partial}{\partial x_i}\left[\left(\mu + \frac{\mu_t}{\sigma_\varepsilon}\right)\frac{\partial \varepsilon}{\partial x_i}\right] + C_{1\varepsilon}\frac{\varepsilon}{k}(G_k + C_{3\varepsilon}G_b) - C_{2\varepsilon}\rho\frac{\varepsilon^2}{k} \tag{10}$$

In the above transport equations, G_k represents the generation of turbulent kinetic energy from mean velocity gradients while G_b is the generation of turbulent kinetic energy from buoyancy. $C_{1\varepsilon}$, $C_{2\varepsilon}$, and $C_{3\varepsilon}$ are constants while σ_k and σ_ε are the turbulent Prandtl numbers for k and ε.

5.2   Model Development

A complete cold plate was modeled within Icepak with three columns and 18 rows of cells to explore the performance of the total unit when only a portion of the cells

experienced degradation. A 3.0 mm thick copper base plate 54.5 mm wide and 239.9

mm long was placed against the cold plate and was given a uniform power

dissipation of 200 W. An isometric view of the cold plate, with the copper base plate

hidden is given in Figure 21.
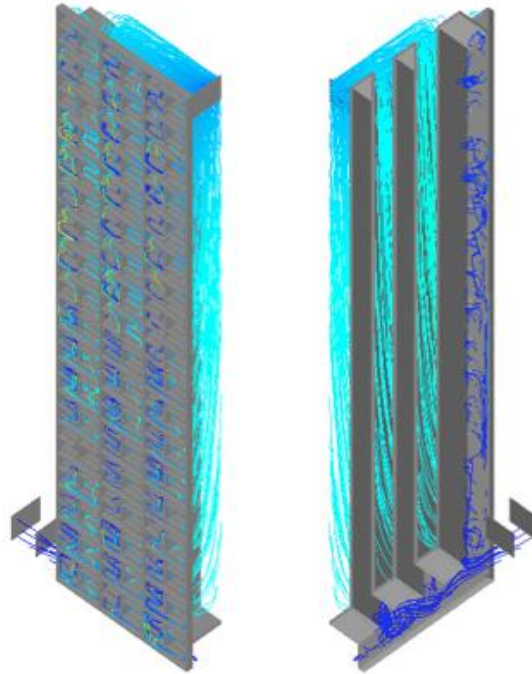
Figure 21. Plastic cold plate model.

A diagram of an individual cell, with dimensions displayed in mm, is shown in Figure

22. All walls have a width of 0.5 mm; external walls and the central vertical wall

have a height of 2 mm while all horizontal internal walls have a of height of 1.8 mm.

The wide channels that connect to the cold plate insert and exit have dimensions of

17.5 mm wide by 12 mm tall. The insert cells were modeled as a polymer with a

thermal conductivity of 0.25 W/m-K.

Figure 22. Individual cell, with dimensions in mm.

Ethylene glycol, 50% by volume with water, was defined as the coolant operating

through the cold plate with the following properties.

Table 7. 50% Ethylene glycol properties.

Volume Expansion (1/K)	0.00048
Dynamic Viscosity (kg/m-s)	0.0046
Density (kg/m^3)	1082.0
Specific Heat (J/kg-K)	3300.0
Conductivity (W/m-K)	0.4
Diffusivity (m^2/s)	1.0
Molecular Weight (kg/kmol)	62.0

The dynamic viscosity and the specific heat capacity properties were refined to be

dependent with temperature, with values shown in Figure 23 and Figure 24 [29].

Figure 23. Dynamic viscosity of 50% ethylene glycol coolant.
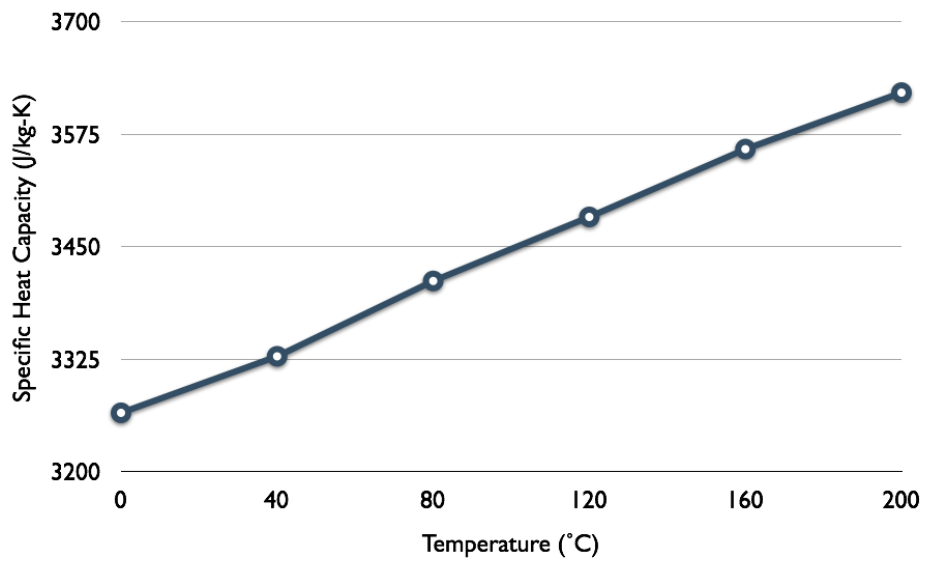
Figure 24. Specific heat of 50% ethylene glycol coolant.

The initial temperature of the coolant was fixed at 20 °C before entering the cold

plate. An exit for the coolant from the unit was specified as an opening at ambient

pressure while a linear pump curve was defined as the entrance; defining a pump

curve instead of a fixed flow provides a more accurate fluid representation when

degradation conditions, such as a blockage of a cell, change the pressure drop across

the unit. The curve allows for a constant pumping power comparison between the reference case and degradation conditions. The linear pump curve was specified as three meters of H_2O at no flow and five LPM at no pressure loss and is pictured in Figure 25.
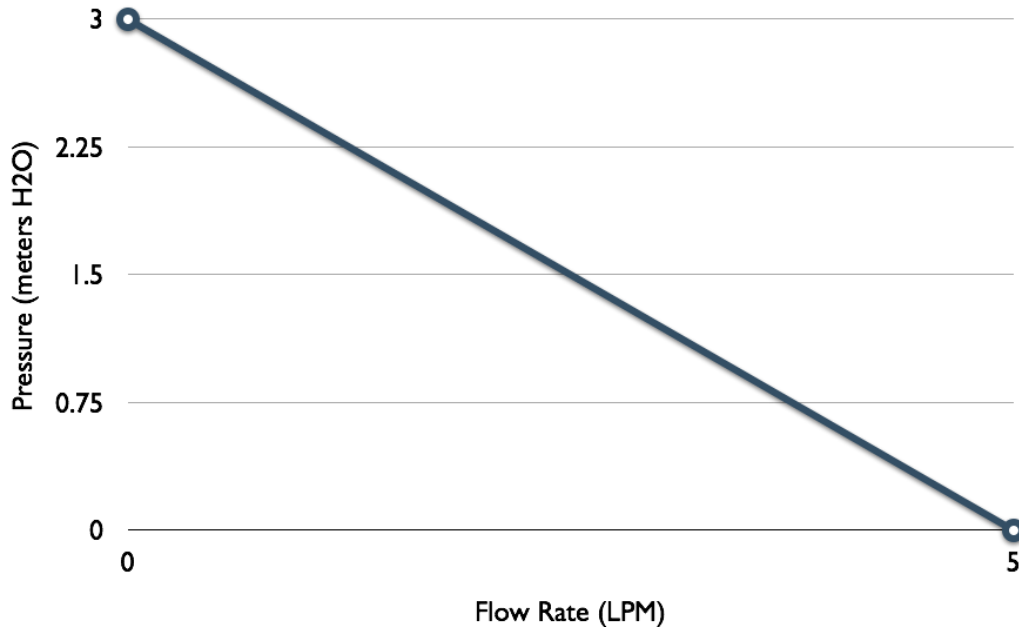
Figure 25. Inlet pump curve.

After the plastic insert cold plate design was modeled in Icepak, the reference simulation was calculated with meshes varying in the total number of elements. An optimum number of elements was found that balanced computational effort with the accuracy of the solution. Four hexahedral meshes of different quality were created by varying the minimum number of elements required in a gap between model objects, the minimum number of elements on each edge of each object, and the maximum ratio of the sizes of adjacent objects. An additional constraint for mesh 2 added that elements could not exceed the dimensions of 2.7, 12, and 0.5 mm

for the X, Y, and Z directions, respectively. A summary of the mesh constraints is

provided in Table 8.

Table 8. Mesh refinement.

	Total Number of Nodes	Minimum Elements in Gap	Minimum Elements on Edge	Max Size Ratio
Mesh 1	228,827	2	1	10
Mesh 2	855,701	2	1	10
Mesh 3	1,041,834	3	2	2
Mesh 4	1,718,930	3	3	2

Each mesh was generated within Icepak and a crossection view was taken to

visualize the size and orientation of the elements within one cell of the plastic

insert. A screenshot of each mesh generated is shown in Figure 26.
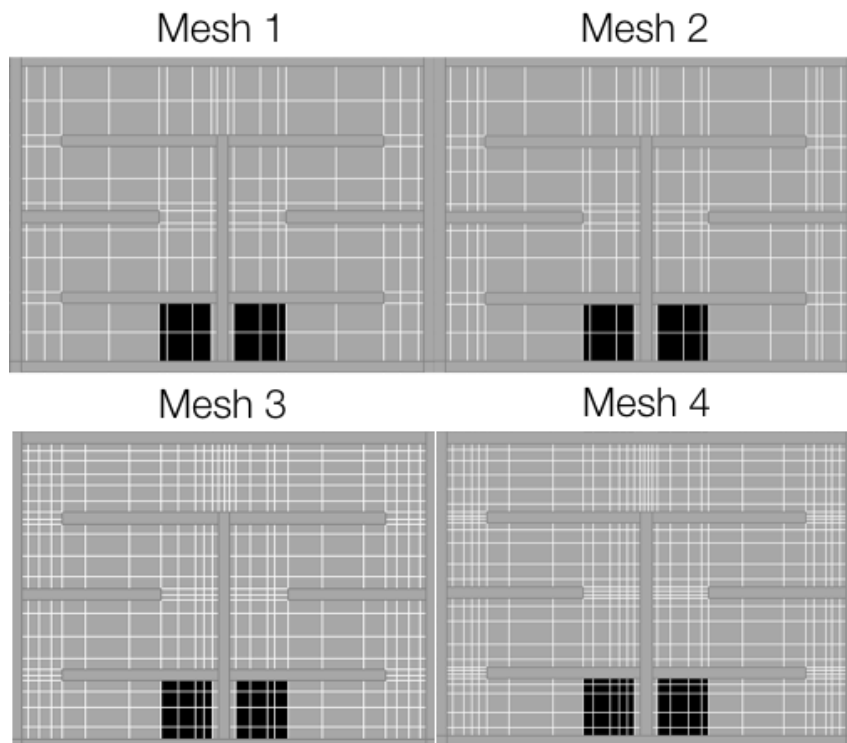
Figure 26. Mesh generation over plastic insert cell.

A solution to each mesh was calculated and the results were validated by qualitatively analyzing streamlines though insert cells and measuring the coolant fluid velocity, temperature, and pressure at several locations along the insert.
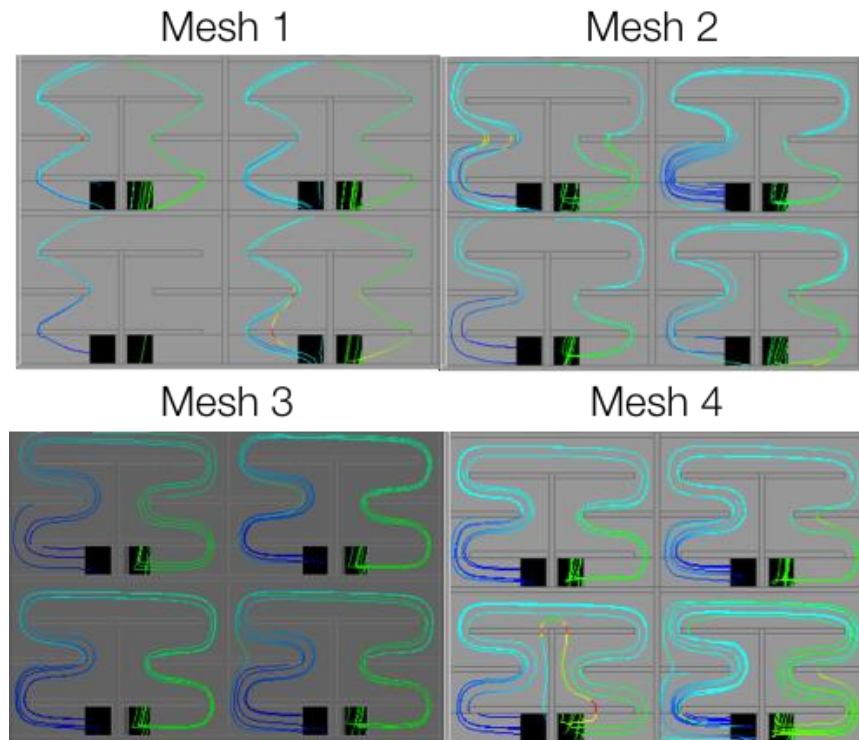
Figure 27. Streamlines through insert cells for various meshes.

Streamlines in each mesh solution, as shown in Figure 27, indicate that mesh 3 and 4 both provide an accurate representation of the coolant flowing through the insert cells. The reduced number of elements in mesh 1 and 2 begin to affect the solution and cause the streamlines to deviate from the higher quality meshes. Eight data locations within the modeled cold plate recorded temperature, pressure, and velocity for each mesh. Measurements at the insert entrance, exit, and within one cell were recorded, as shown at locations in Figure 28.
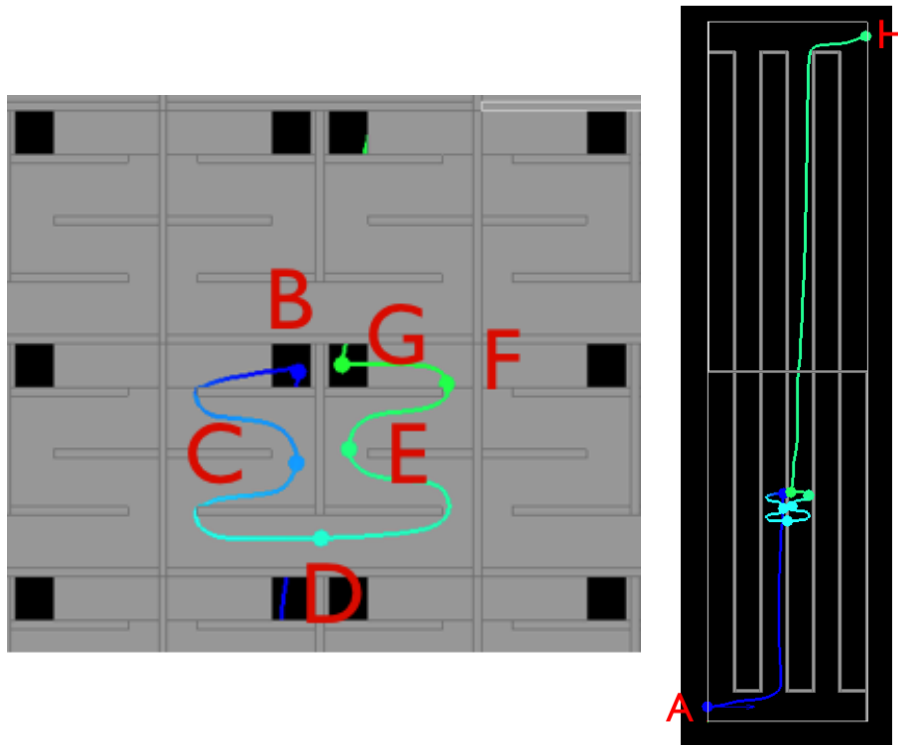
Figure 28. Measurement locations.

The measurements taken at the above locations indicate that mesh 3 and 4 simulate a flow with similar temperature and velocity measurements. Mesh 1 and 2 also provide similar temperature measurements but the velocity measurements varied at most locations compared to mesh 4. A summary of the measurements taken for calibration is provided in Table 9. The results indicated that the decrease in number of elements and computational time from mesh 4 to 3 did not impact the results of the solution. Additional reduction in elements caused noticeable changes in results for meshes 2 and 1, therefore mesh 3 was selected as the optimal level of quality for all following degradation cases.

Table 9. Mesh calibration measurements.

	Mesh	A	B	C	D	E	F	G	H
Temperature (°C)	1	20.00	20.13	21.38	22.05	22.74	22.91	22.74	22.80
	2	20.00	20.11	21.11	21.82	22.41	22.73	22.73	22.78
	3	20.00	20.08	21.13	21.92	22.41	22.74	22.94	22.80
	4	20.00	20.07	21.12	21.87	22.42	22.74	22.94	22.79
Pressure (N/m²)	1	235.46	227.51	175.44	134.81	93.74	63.98	45.32	3.04
	2	270.11	257.00	200.96	152.71	103.03	68.14	50.68	3.14
	3	258.31	248.83	194.19	145.70	98.63	64.71	47.50	2.47
	4	266.18	255.88	199.88	150.08	101.10	67.08	47.97	2.41
Velocity (m/s)	1	0.1667	0.0465	0.0303	0.0174	0.0314	0.0189	0.0481	0.0163
	2	0.1667	0.0462	0.0843	0.0668	0.0860	0.0656	0.0484	0.1481
	3	0.1667	0.0721	0.0890	0.0898	0.0905	0.0700	0.0853	0.0176
	4	0.1667	0.0744	0.0922	0.0889	0.0896	0.0838	0.0862	0.0247

The velocity measurements recorded above, along with previously listed fluid properties and insert geometry, allow for the Reynolds number in various channel locations to be calculated by the following equation for a pipe or duct.

$$Re = \frac{\rho V D_H}{\mu} \tag{11}$$

where

ρ = density of the fluid (kg/m³)

V = fluid velocity (m/s)

D_H = hydraulic diameter of the channel, equal to four times the cross-sectional area, divided by the wetted perimeter (m)

μ = dynamic viscosity of the fluid (kg/m-s)

Measurements at locations A, B, and D represent the wide channel region, cell entrance region, and cell channel region, respectively. Reynolds numbers for each location was calculated to be 558, 42, and 51 for each region, showing that the fluid flow in the plastic insert is well within the laminar region.

5.3 Reference and Degradation Conditions

The reference case was modified slightly from the optimization cases to more closely model a typical medium power application. For a 600 V, 200 A IGBT module operating at 98% efficiency, 2,400W would need to be dissipated by the cold plate. This was modeled as a uniform heat flux over the copper base plate. The inlet coolant temperature was also raised from 20 ℃ to 60 ℃. In addition to the reference case, the following long term degradation conditions were explored:

- Cell blockage – A full blockage of a cell could occur from the lodging of a particle from the coolant into a cell's entrance or exit. This could also occur by gradual buildup of smaller particles clumping together. A full cell blockage was modeled by completely sealing off the entrance and exit openings of four adjacent cells.

- Partial blockage – Before full blockage of a cell occurs, partial blockages can occur in the cell's openings and along its internal walls. The internal walls within a cell are configured to direct the coolant in a serpentine flow, but do not fully extend to the face of the copper base plate. This creates a region where a small fraction of coolant can pass over the top of the walls; as a result, pressure drop over the cell decreases and thermal performance is also improved [9]. A partial blockage was modeled as the fouling of this 0.2 mm gap in all internal walls of each cell.

- Cell opening – Erosion of cell features from particles in the coolant was viewed as a possible long term wear out mechanism. An alteration in coolant flow amount or path would alter the thermal performance of a

cell from its original design. Three opening conditions were modeled, enlargement of the inlets and outlets by 3 mm, enlargement of the gap between internal walls and the base plate by 0.2 mm, and shortening of the internal walls by 2 mm. Each condition was applied to every cell in the plastic insert.

- Coolant degradation – Previous analysis of used coolant found that the percentage of ethylene glycol rose from 50% to 60%, causing viscosity to increase and the specific heat capacity to decrease. The coolant properties in the model were altered to reflect the higher concentration of glycol.

Visual examples of these cell degradation conditions with coolant streamlines are shown in Figure 29.
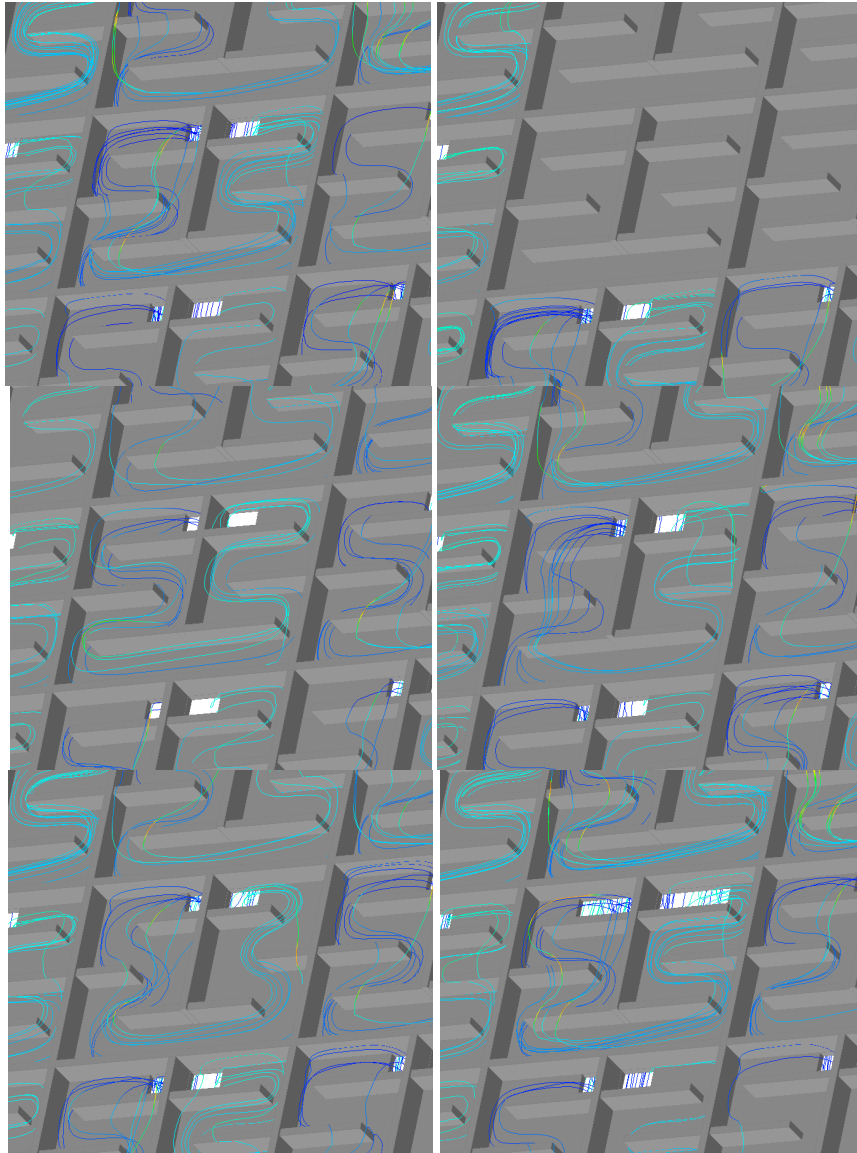
Figure 29. Degradation conditions. Clockwise from top left: reference case, four blocked cells, lower cell walls, larger inlets/ outlets, shorter cell walls, higher cell walls.

In the same procedure as mesh refinement, eight data locations within the modeled

cold plate recorded temperature, pressure, and velocity for each mesh, listed in

Table 10.

Table 10. Degradation condition measurements.

	Condition	A	B	C	D	E	F	G	H
Temperature (°C)	Reference Case	60.10	60.37	62.82	67.40	68.58	70.70	70.70	66.03
	Blockage, Four Cells	60.10	60.37	62.82	67.40	68.58	70.70	70.70	66.03
	Partial Blockage, Higher Walls	60.20	60.63	64.04	66.14	68.80	71.46	70.99	62.34
	Cell Opening, Lower Walls	60.11	60.33	61.73	65.54	67.24	69.09	70.78	65.81
	Cell Opening, Shorter Walls	60.02	60.07	61.11	64.82	65.89	66.04	66.72	66.26
	Cell Opening, Inlet/Outlet	60.10	60.37	62.82	67.40	68.58	70.70	70.70	66.03
	60% Ethylene Glycol	60.19	60.56	63.40	68.34	69.61	72.01	70.88	63.51
Pressure (N/m²)	Reference Case	6861	4393	4197	4087	3992	3910	3850	172
	Blockage, Four Cells	6861	4393	4197	4087	3992	3910	3850	172
	Partial Blockage, Higher Walls	7611	4793	4464	4296	4148	3991	3902	170
	Cell Opening, Lower Walls	7423	4474	4321	4250	4197	4166	4063	161
	Cell Opening, Shorter Walls	10457	6609	6310	6091	6023	5925	5656	217
	Cell Opening, Inlet/Outlet	6861	4393	4197	4087	3992	3910	3850	172
	60% Ethylene Glycol	6703	4538	4327	4222	4133	4055	3977	147
Velocity (m/s)	Reference Case	0.2811	0.1033	0.1836	0.1757	0.1901	0.1389	0.1358	0.0734
	Blockage, Four Cells	0.2811	0.1033	0.1836	0.1757	0.1901	0.1389	0.1358	0.0734
	Partial Blockage, Higher Walls	0.2824	0.2088	0.2297	0.1568	0.2392	0.1508	0.2267	0.0664
	Cell Opening, Lower Walls	0.2915	0.1774	0.1405	0.1771	0.1397	0.1057	0.2312	0.0757
	Cell Opening, Shorter Walls	0.5894	0.2757	0.1053	0.2575	0.1380	0.1505	0.3541	0.0893
	Cell Opening, Inlet/Outlet	0.2811	0.1033	0.1836	0.1757	0.1901	0.1389	0.1358	0.0734
	60% Ethylene Glycol	0.2384	0.0648	0.1796	0.1666	0.1854	0.1337	0.1478	0.0729

Degradation of the coolant was modeled by changing ethylene glycol properties from 50% to 60% concentration, as listed in Table 11. Dynamic viscosity and specific heat were refined to be dependent with temperature by the same method as 50% properties [29].

Table 11. 60% ethylene glycol properties.

Property	50%	60%
Volume Expansion (1/K)	0.00048	0.00052
Dynamic Viscosity (kg/m-s)	0.0046	0.0053
Density (kg/m^3)	1082.0	1098.0
Specific Heat (J/kg-K)	3300.0	3100.0
Conductivity (W/m-K)	0.4	0.38
Diffusivity (m^2/s)	1.0	1.0
Molecular Weight (kg/kmol)	62.0	62.0

After convergence to a steady state solution for each degradation condition,

temperature profiles of the copper base plate were analyzed. The maximum,

minimum and average temperatures of the top surface of the base plate were

determined and the temperature rise for each degradation condition is provided in

Table 12.

Table 12. Comparison of temperature rise under degradation conditions.

	Min. Temp. (˚C)	Max. Temp. (˚C)	Mean Temp. (˚C)
Reference Case	92.9	96.4	94.8
Blockage, Four Cells	92.9	96.4	94.8
Partial Blockage, Higher Walls	136.3	139.0	138.0
Cell Opening, Lower Walls	101.0	104.6	103.0
Cell Opening, Shorter Walls	89.1	91.9	90.7
Cell Opening, Inlet/Outlet	92.9	96.4	94.8
60% Ethylene Glycol	96.0	100.1	98.3

The model shows that a plastic-insert cold plate design can adequately cool a base

plate with a uniform heat flux of 2,400 W. Introducing degradation conditions to the

insert creates a varied response in base plate temperatures. Modification of the cell

inlets and outlets, by blockage of four adjacent cells or enlargement of all cell

openings, showed no alteration in the temperature rise of the base plate. The

removal or enlargement of the 0.2 mm internal wall gap caused the largest

alteration in cold plate performance and increase in base plate temperature, indicating that the reference case wall height was optimal. Shortening the length of the internal walls proved to be advantageous as base plate temperatures were reduced from the reference case geometry. Diminished heat capacity of the coolant to a 60% ethylene glycol ratio caused the temperatures of the copper block to rise. Analysis of the cold plate's ability to keep a power module within manufacturer's recommended operation temperatures is continued when geometry and heat fluxes are specified for IGBTs and diodes.

5.4   Rise in Power Electronics Temperature

The previous analysis provided information on the rise in copper block base plate temperature for a uniform heat flux under a variety of degradation conditions. The thermal resistance of a typical power electronics package can be calculated to determine the temperature of the IGBT under degradation conditions. A cross section of a package is provided in Figure 30, including layer thicknesses [30].

Figure 30. Layer materials and thicknesses in power electronics module.

The Ohm's law of thermal circuits is a method that describes heat dissipation from an IGBT by the concept of thermal resistance, where heat transfer is described in a similar manner as the transmission of electricity. Ohm's law states that for electricity, voltage equals the product of current flow and resistance. The thermal analogy is that a temperature drop, ΔT, is equal to the heat flow, q, multiplied by the thermal resistance, R_{therm} [31].

$$\Delta T = qR_{thern} \text{ where } \Delta T = T_1 - T_2 \text{ and } T_1 > T_2 \qquad (12)$$

The thermal resistance for conduction through a plane wall can be found by rearranging the above equation, where resistance, R, equals the thickness, t, of the material divided by the product of thermal conductivity, k, and area, A.

$$R_{cond} = \frac{T_1 - T_2}{q} = \frac{t}{kA} \qquad (13)$$

The thermal resistance of each layer in the power electronics package can be calculated and summed to find the equivalent thermal resistance network. The area of the IGBT (9.78 mm x 13.72 mm) was used as the area for the first layer. Heat spreads through materials at a spreading angle, increasing the area value for each layer. The angle of thermal spreading and the surface length for each layer is found by the following equations [32].

$$\alpha_a = tan^{-1}\left(\frac{k_a}{k_b}\right)$$ (14)

$$L_2 = 2t_a tan(\alpha_a) + L_1$$ (15)

where

α_a = angle of thermal spreading through material a (K)

k_a = thermal conductivity of material a (W/m-K)

k_b = thermal conductivity of material b (W/m-K)

L_1 = length of thermal effect at interface 1 (m)

L_2 = length of thermal effect at interface 2 (m)

Each layer's thickness and thermal conductivity are provided in Table 13, along with the angle of thermal spreading and the surface length of the thermal effect. The material conductivity value of the solder was considered to be from a lead free 3.5 Ag, 96.5 Sn composition [33]. Other materials included silicon for the IGBT and copper and alumina for the DBC [34].

Table 13. Thermal surface length calculation.

Layer	Material	Thickness (mm)	Conductivity (W/m-K)	Alpha (°)	Length (mm)	Width (mm)
IGBT	Silicon	0.09	150	77.59	13.72	9.78
Solder	3.5 Ag 96.5 Sn	0.127	33	4.72	14.54	10.60
DBC Top Layer	Copper	0.31	400	86.57	14.56	10.62
DBC Substrate	Al_2O_3 96%	0.625	24	3.43	24.89	20.95
DBC Bottom Layer	Copper	0.31	400	85.28	24.97	21.03
Solder	3.5 Ag 96.5 Sn	0.127	33	4.72	32.48	28.54
Base Plate	Copper	3	400		-	

The cross-sectional area is not constant for each layer because of the spreading effect, therefore the average area can be found by finding the average length of effect in a layer.

$$L_{aAVG} = \frac{L_2 - L_1}{2} + L_1 \tag{16}$$

$$A_{aAVG} = L_{aAVG}{}^2 \tag{17}$$

In the case of the given IGBT, the length and width have different dimensions and are multiplied together. The average length, width, area, and total package thermal resistance are provided in Table 14.

Table 14. Thermal resistance calculation.

Layer	Average Length (mm)	Average Width (mm)	Average Area (mm²)	Resistance (K/W)
IGBT	13.72	9.78	134.18	0.0045
Solder	14.13	10.19	143.96	0.0267
DBC Top Layer	14.55	10.61	154.34	0.0050
DBC Substrate	19.73	15.79	311.39	0.0836
DBC Bottom Layer	24.93	20.99	523.28	0.0015
Solder	28.54	24.79	711.95	0.0054
Total Resistance to Base Plate				0.1267

The total thermal resistance from the IGBT to the top of the copper base plate was found to be approximately 127 K/kW. Measurement of the heat breakdown for an IGBT and diode pair with the above specifications for an automotive application estimated a heat loss of 120 W [30]. The estimated heat breakdown between components proportioned approximately 70% of the heat to the IGBT, for a total heat loss of 85 W. By equation 11, the temperature drop from the IGBT to the top of the copper base plate can be calculated.

$$\Delta T = qR_{therm} = (85W) \cdot (0.1267K/W) = 10.14K \qquad \textbf{(18)}$$

This temperature drop of 10.14 K can be added to the previous base plate temperatures to find the maximum IGBT operating temperature for the reference case and each degradation condition, shown in Table 15.

Table 15. Maximum IGBT temperatures.

	Max. Base Plate Temp. (℃)	Max. IGBT Temp. (℃)
Reference Case	96.4	107.2
Blockage, Four Cells	96.4	107.2
Partial Blockage, Higher Walls	139.0	149.8
Cell Opening, Lower Walls	104.6	115.4
Cell Opening, Shorter Walls	91.9	102.7
Cell Opening, Inlet/Outlet	96.4	107.2
60% Ethylene Glycol	100.1	110.9

Commercially available IGBT modules are designed to operate up to junction temperatures of 150 ℃. The calculated IGBT temperatures indicate that blockage of the 0.2 mm internal wall gap would cause the power module to approach this design rating. The reference case and other degradation conditions do not exceed the maximum junction temperature specification. Elevated temperatures can still result in decreased reliability.

Chapter 6: Conclusions, Contributions, and Future Work

6.1 Conclusions

This thesis provides a holistic review of the concerns associated with a single-phase liquid cooling system. The novel concept of a plastic insert allows for a reduction in thermal gradients across a cold plate and can allow for designs more tailored to applications than traditional metal cold plates. The use of a new design and materials first requires a thorough reliability evaluation before the concept can be implemented into production. Material analysis of the plastic insert and elastomer seal were completed, as well as compression set testing of EPDM in ethylene glycol at various elevated temperatures. Used coolant testing found that most parameters were within specification of new coolant; elevated percentages of glycol were found to decrease the heat transfer ability of the fluid. A CFD analysis of the plastic insert cold plate assembly evaluated various degradation conditions and allowed for the IGBT chip temperature to be calculated while being cooled by a suboptimal cold plate.

Common elastomer materials were evaluated under several chemical and thermal requirements, including compatibility with ethylene glycol and water at elevated temperatures and degradation free performance at temperatures from -40 ˚C to 125 ˚C. Ethylene propylene diene, silicone, and fluorosilicone met these requirements with fluorosilicone being the most suitable if compatibility with fuel oils was added as an additional requirement.

A similar polymer analysis required the plastic insert to be molded from a material that exhibits no effect when in contact with ethylene glycol, minor to no effect with fuel oils, and minimal absorption of water. The heat deflection temperature and maximum continuous operating temperature were also used to conclude that polyether ether ketone (PEEK), polyphenylene sulfide (PPS), and polyvinylidene fluoride (PVDF) meet the design requirements.

Compression set testing of EPDM 70A durometer material by ASTM D-395 Method B standard was completed to find any effects of EPDM submerged in ethylene glycol at elevated temperatures. Samples reduced to 75% of their original thickness for 72 hours revealed a linear relationship of increasing level of compression set with increasing temperature. Concerns about leakage were alleviated as the experimental results match documented compression set levels for EPDM.

An organic acid technology (OAT) antifreeze was analyzed from new samples as well as from samples that had been used for three years. Comparisons to acceptable parameters were made for color change, density, pH, conductivity, kinematic viscosity, freezing point, ethylene glycol percentage, and boiling point. A higher than expected ethylene glycol percentage lowered the coolant's freezing point, but more importantly reduced the specific heat capacity of the coolant.

A model of the plastic insert cold plate was designed in the CAE software Icepak for various degradations of the plastic insert and coolant to be modeled. A reference case of cooling a copper base plate with a uniform heat flux of 2,400 W was established before degradation conditions were explored. After the maximum

temperatures of the copper base plate were found, a thermal resistance network of an IGBT power module was calculated to determine the module's junction temperature. Only one degradation case, blockage of the 0.2 mm internal wall gap, was found to cause the power module to closely approach its maximum operating temperature rating.

6.2   Contributions

The major contributions provided by this work are as follows:

- Material evaluation and selection of compatible elastomers for seals and polymers for a plastic insert cold plate design.
- Compression set testing confirming the minimal impact of ethylene glycol coolant on selected EPDM seal material.
- Evaluation of used coolant for additional degradation conditions in the thermal management system.
- CFD analysis of a plastic insert cold plate for various wear out or fouling conditions and a corresponding IGBT maximum operating temperature.

6.3   Future Work

The following are suggestions for future work:

- Validation of the Icepak developed model with an experimental setup would provide correlations between simulated degradations and wear out mechanisms from a physical cold plate.

- Reliability analysis could be expanded to an analysis of all critical components within a coolant loop, such as the radiator or circulating pump.

- Additional information by a manufacture on unscheduled repair history could highlight additional degradation methods within the cooling system.

Works Cited

[1] H. Bullinger, *Technology Guide: Principles, Applications, Trends.* Springer, 2009. ISBN 978-3-540-88545-0. Chap 2, p. 78-83.

[2] M. Olszewski, "Evaluation of the 2007 Toyota Camry Hybrid Synergy Drive System," Oak Ridge National Laboratory, 2008.

[3] K. Meyyappan, P. McCluskey, "Virtual Qualification of Power Components and Modules," CALCE EPSC, University of Maryland.

[4] W. Sheng, R. Colino, *Power Electronic Modules: Design and Manufacture.* CRC Press, 2005. ISBN 978-0849322600.

[5] P. Hansen, P. McCluskey, "Failure models in power device interconnects," Power Electronics and Applications, 2007.

[6] E. de Vries, 2004, "Mechanics and Mechanisms of Ultrasonic Metal Welding," Ph.D. Thesis, Ohio State University, Columbus, Ohio.

[7] S. Kandlikar, C. Hayner II, "Liquid Cooled Cold Plates for Industrial High-Power Electronic Devices—Thermal Design and Manufacturing Considerations," Heat Transfer Engineering, vol. 30, no. 12, pp. 918-930, 2009.

[8] "Inverter Mechanical Disassembly," Techno Fandom. Available: http://www.techno-fandom.org/~hobbit/cars/ginv/i1mech.html

[9] Olesen, K., Bredtmann, R., Eisele, R., "'ShowerPower' New Cooling Concept for Automotive Applications," Automotive Power Electronics, Paris, 21-22 June 2006.

[10] B. Williams, *Principles and Elements of Power Electronics: Devices, Drivers, Applications, and Passive Components,* Barry W. Williams, 2006. ISBN 978-0-9553384-0-3.

[11] "O-ring and Seal Failure Analysis." PSP Global. Available: http://www.pspglobal.com/seal-failure.html

[12] "Compounds for Nitrile O-Rings (Buna n)." PSP Global. Available: http://www.pspglobal.com/nitrile-buna-n.html

[13] "Types of Neoprene – Dry Rubber Applications." DuPont Performance Elastomers. Available: http://www.dupontelastomers.com/literature/neoprene/585E7A59DA93810F6B1A7900D3712585.pdf

[14] "Kalrez® O-Rings and Seals." PSP Global. Available:
http://www.pspglobal.com/kalrez-o-rings/index.html

[15] "Chemical Resistance and Fluid Compatibility, Including All Chemicals Under the Clean Air Act." DuPont Dow Elastomers. Available:
http://dymseal.com/pdf/090017a280061ed8.pdf

[16] G. Holden, H. Kricheldorf, R. Quirk. *Thermoplastic Elastomers, Third Edition*. Hanser, 2004. ISBN 3-446-22375-4.

[17] "Compatibility." O-Rings Inc. Available:
http://www.oringsusa.com/html/compatibility.html

[18] "O-Ring Materials Compatible with Chemical Ethylene Glycol." eFunda Inc. Available:
http://www.efunda.com/designstandards/oring/oring_chemical.cfm?SM=none&SC=Ethylene%20Glycol

[19] C. MacDermott, A. Shenoy. *Selecting Thermoplastics for Engineering Applications, Second Edition*. Marcel Dekker, New York, 1997.

[20] "Material Selection Guide." Boedeker. Available:
http://www.boedeker.com/mguide.htm

[21] "O-ring Failure Analysis." All Orings. Available:
http://www.allorings.com/failure.htm

[22] "Operating Temperature of Plastics." Dotmar Engineering Plastic Products. Available: http://www.dotmar.com.au/operating-temperature.html

[23] *Annual Book of ASTM Standards* 2006. ASTM International. Section Nine Rubber vol. 09.01, pp. 38-43, 2006.

[24] H. Phlegm, *The Role of the Chemist in Automotive Design,* CRC Press, 2009. ISBN 978-1-4200-7188-7.

[25] "MSDS TEXACO Havoline DEX-COOL Extended Life Anti-Freeze/Coolant." Chevron Texaco. Available:
http://www.havoline.com/images/products/pdfs/anti_exlife.pdf

[26] "Coolant Analysis Interpretation Guide." The Fluid Life Corporation. Available:
http://www.fluidlife.com/media/pdfs/coolant_interpretation_guide.pdf

[27] *Icepak 4.4 User's Guide.* Fluent Inc. 2007.

[28] G. K. Batchelor. *An Introduction to Fluid Dynamics*. Cambridge Univ. Press, Cambridge, England, 1967.

[29] "Ethylene Glycol Heat-Transfer Fluid." The Engineering Toolbox. Available: http://www.engineeringtoolbox.com/ethylene-glycol-d_146.html

[30] M. O'Keefe, A. Vlahinos. "Impacts of Cooling Technology on Solder Fatigue for Power Modules in Electric Traction Drive Vehicles," IEEE Vehicle Power and Propulsion Systems Conference, 2009.

[31] F. Incropera, D. DeWitt, *Fundamentals of Heat and Mass Transfer, 5th Edition*. Wiley, 2001. ISBN 978-0471386506.

[32] R. Ulrich, W. Brown, *Advanced Electronic Packaging, 2nd Edition.* Wiley-Interscience, 2006. ISBN 978-0-47146609-X, p. 573-575.

[33] "Lead Free Solder Alloys." Williams Advanced Materials. Available: http://www.williams-adv.com/packagingMaterials/lead-free-solder.php

[34] C. Zweben, "Composite Materials And Mechanical Design", *Mechanical Engineers' Handbook, Second Edition.* M. Kutz, Ed, John Wiley & Sons, Inc., New York, 1998. ISBN 978-0471130079.